Synchronization challenges in deep space communications

Jordi Vilà-Valls, Monica Navarro, Pau Closas, Massimo Bertinelli

DOI. No. 10.1109/MAES.2019.170208

Feature Article:

Synchronization Challenges in Deep Space Communications

***Jordi Vilà-Valls, Monica Navarro*, Centre Tecnològic de Telecomunicacions de Catalunya, Barcelona, Spain**
***Pau Closas*, Northeastern University, Boston, MA, USA**
***Massimo Bertinelli*, European Space Agency, Noordwijk, The Netherlands**

INTRODUCTION

Deep space missions keep pushing for new frontiers affecting a wide spectrum of disciplines. To support the scientific achievements expected from new missions, communication technology is being pushed towards its limits [1]. A need to increase communication links data rate as well as to lower the operative signal-to-noise ratio (SNR) are identified. The adoption of advanced coding schemes such as turbo codes and low-density parity-check (LDPC) codes (e.g., Consultative Committee for Space Data Systems (CCSDS) standards) allows receivers to operate at lower SNRs. However, in order to exploit the full potential of the coding gain, the receiver must be able to acquire and track a signal with a SNR much lower than expected in nominal conditions of state-of-the-art systems. The target operating point is given by the candidate LDPC codes [2], where the codeword error rate is set to WER $\leq 10^{-5}$, achieved at the bit energy to noise density ratio $E_b/N_0 \geq 5.2$ dB, ≥ 3.6 dB for LDPC(128,64) and LDPC(256,128), respectively. In [3] the first receiver bottleneck related with frame synchronization, a functionality required previous to channel decoding, was identified. Even though frame synchronization enhancements were proposed beyond standard correlation techniques [3], [4], [1], it was recommended to increase the synchronization word length in order to achieve the target performance. The recommendation was recently adopted by the CCSDS. In this work, the focus lies on the receiver synchronization stages (i.e., acquisition and tracking). Not only from a research standpoint, but also for the design of next generation Telemetry Tracking & Command (TT&C) transponders, it is of capital importance to understand the performance limitations of state-of-the-art deep space communications architectures, clearly identifying possible bottlenecks and the synchronization stages (i.e., acquisition and tracking) to be improved. Digital carrier and timing synchronization have been an active research field for the past three decades in applications such as satellite-based positioning or terrestrial wireless communications systems. In those scenarios, the limitations of standard delay, frequency, and phase-locked loop (delay-locked loop, frequency-locked loop (FLL), and phase-locked loop (PLL), respectively) architectures have been clearly overcome by Kalman filter (KF) based solutions [5], which provide an inherent adaptive bandwidth, robustness, flexibility, and an optimal design methodology. Despite the advances in the field, synchronization architectures for deep space communications links, implemented in current TT&C transponders, still rely on well-known conventional architectures, which may be insufficient if limits are pushed to extremely low SNR or harsh propagation conditions. With the advent of powerful software defined radio receivers and new system design rules, it is now possible to adopt new robust architectures that may enable going beyond the performance and reliability provided by legacy solutions.

This contribution deals with the synchronization problem in deep space telecommand (TC), much more challenging in terms of system requirements than its telemetry counterpart, due to onboard processing and implementation constraints. First, we provide a thorough analysis to identify the performance limits of standard synchronization techniques; then, we show the possible performance improvements (and limitations) of innovative state-of-the-art acquisition and tracking architectures. Namely, we discuss: (i) fast Fourier transform (FFT)-based carrier acquisition, (ii) FLL-assisted PLL and KF-based carrier tracking schemes, (iii) FFT-aided subcarrier tracking, (iv) coherent carrier/subcarrier tracking, and (v) noncoherent timing synchronization to avoid the subcarrier stage.

SIGNAL MODEL

Deep space communication, and in particular planetary exploration missions, require dealing with signals, such as in the telecommand link, with a very low SNR. In this case, the signal is generated by modulating a carrier with a subcarrier, in turn modulated by data. The resulting modulation, entailing a residual carrier, is commonly referred to as pulse code modulation (PCM)/phase-shift keying (PSK)/phase modulation (PM) [6]. The real-valued passband model for the transmitted signal is given by,[1]

Authors' current addresses: J. Vilà-Valls, M. Navarro, Statistical Inference for Communications and Positioning Department, Centre Tecnològic de Telecomunicacions de Catalunya (CTTC/CERCA), 08860, Barcelona, Spain, E-mail: ({jvila, mnavarro}@cttc.cat). P. Closas, Northeastern University, Boston, MA, USA. M. Bertinelli, European Space Agency, Noordwijk, The Netherlands.

Review handled by D. Ciuonzo.

[1] This signal (1) usually includes a ranging component, but it was excluded since it was irrelevant for this work.

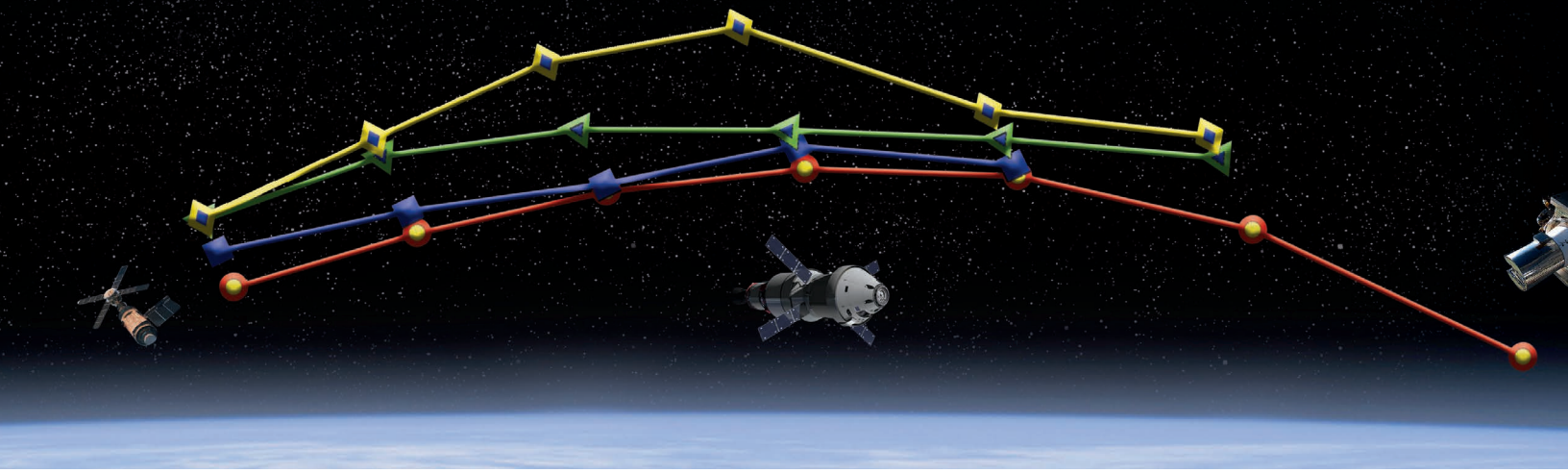

$$s(t) = A\sin\left(2\pi f_c t + m_c d(t)\sin\left(2\pi f_{sc} t + \phi_{sc,0}\right) + \phi_{c,0}\right), \quad (1)$$

where A is the signal amplitude, f_c is the carrier frequency, $\phi_{c,0}$ is the initial carrier phase, m_c denotes the modulation index (i.e., $0.2 \le m_c \le 1.4$), f_{sc} is the subcarrier frequency, $\phi_{sc,0}$ is the initial subcarrier phase, and $d(t)$ is the information data stream non return to zero-level (NRZ-L) PCM encoded as,

$$d(t) = \sum_k c_k p_{\mathrm{NRZ}}(t - kT_b), \quad (2)$$

with $c_k \in \{-1, 1\}$, T_b the symbol period, and p_{NRZ} the pulse waveform,

$$p_{\mathrm{NRZ}} = \begin{cases} 1 & t \in [0, T_b) \\ 0 & \text{otherwise} \end{cases}. \quad (3)$$

The data rates are in the range 7.8125 sps $\le R_s \le$ 4 ksps (i.e., $4{,}000/2^n$ with n = 0, 1, …, 9). The standard establishes that the subcarrier frequency (8 or 16 kHz) shall be an integer multiple of the symbol rate. Furthermore, the data stream and subcarrier waveform shall be coherent in time with coincident zero-crossing, that is, $\phi_{sc,0} = 0$. The equivalent complex-baseband signal $x(t)$ is

$$x(t) = x_I(t) + jx_Q(t), \quad (4)$$

related to the real-valued pass-band signal by

$$s(t) = \Re\left\{x(t)e^{j2\pi f_c t}\right\}, \quad (5)$$

where $x_I(t)$ and $x_Q(t)$ are the real and imaginary parts, respectively. They can be written as,

$$x_I(t) = Ad(t)\sin\left(m_c \sin\left(2\pi f_{sc} t\right)\right), \quad (6)$$

$$x_Q(t) = -A\cos\left(m_c \sin\left(2\pi f_{sc} t\right)\right), \quad (7)$$

where the in-phase component contains the data-bearing signal and the quadrature component contains the residual carrier.

The received signal $r(t)$, which includes the channel propagation impairments, as well as noisy effects introduced by the receiver, is modeled as an additive white Gaussian noise channel in presence of Doppler and phase noise,

$$r(t) = x(t)e^{j\phi_d(t) + \phi_{\mathrm{noise}}} + n(t), \quad n(t) \sim \mathcal{CN}\left(0, \sigma_n^2\right), \quad (8)$$

with $\phi_d(t)$ the phase evolution associated to the Doppler dynamics and ϕ_{noise} the phase noise. Note that the initial carrier phase is included in the carrier phase contribution introduced by the channel model, ϕ_{noise}. Additionally, we may have a possible Doppler impact on the data, which has a similar effect as a clock jitter (in terms of sampling jitter). That is, time between signal samples is not constant, affecting the actual symbol period. In a discrete-time signal model, the effect is that the number of samples per symbol varies over time. This effect is known as incommensurate sampling and is not taken into account. It is considered a negligible effect because we can assume a quasi-analog sampled signal commonly available in state-of-the-art transponders, i.e., several thousand times higher than the symbol rate. Also, we may consider the Doppler effect in the subcarrier frequency. We can easily take this effect into account by adding an additional term to the nominal subcarrier frequency as $\tilde{f}_{sc} = f_{sc} + \delta f_{sc}$.

A list of parameters for a representative deep space communications scenario is summarized in Table 1.

Table 1.

Parameters Specifications for a Reference Deep Space Communications Scenario

Parameters	Deep Space Scenario (e.g., Exomars Mission)
Modulation type	Remnant carrier
Waveform	PCM NRZ-L; sine-waveform sc
Modulation index	m_c = 1.2 rad
Symbol rate	R_s = 7.8125 sps to 4 ksps
Carrier freq.	f_c in X-band
Subcarrier freq.	f_{sc} = 8 or 16 kHz
Uplink f_c	7145-7190 MHz
Real Doppler on f_c	± 400 kHz
Compensated Doppler	± 2 kHz
Doppler on f_{sc}	±1 Hz

TYPICAL DEEP SPACE TELECOMMAND RECEIVER ARCHITECTURE

The block diagram of a typical deep space TC receiver is shown in Figure 1. Note that for the sake of clarity, the complex signal modeling is used instead of the quadrature (I&Q) signal decomposition with real and imaginary parts. The transponder is configured to receive a PCM/PSK/PM signal. In this configuration, a subcarrier tracking loop (implemented as a Costas loop) is in place.

CARRIER ACQUISITION

The carrier acquisition scheme is based on the carrier sweeping algorithm at the sending end (ground station) and a second order PLL at the receiver end, with an atan2 discriminator. The PLL error signal will most likely show an erratic behaviour until the swept carrier enters the pull-in range of the tracking loop. Then, if properly adjusted, the PLL will lock to the signal.

CARRIER PHASE TRACKING

Once the carrier frequency is acquired the receiver enters the carrier tracking loop, which implements the same second order PLL initialized to the resting frequency acquired in the previous stage (a higher order filter may also be considered). In this stage, the receiver could eventually reduce its loop bandwidth since the carrier frequency change rate is only due to the spacecraft dynamics, while in the previous stage the change rate is given by the sum of sweep and Doppler rate.

SUBCARRIER PHASE TRACKING

In the presence of a modulated subcarrier, as is the case for deep space scenarios, a subcarrier acquisition and tracking stage follows the second order PLL. The baseline algorithm is a second order Costas-loop with an atan discriminator. The block diagram is depicted in Figure 1, where the subcarrier switch has to be turned on before passing the signal to symbol timing and demodulation. This module needs to cope with additional Doppler on the subcarrier, not compensated by the PLL on the carrier signal.

SYMBOL-TIMING TRACKING

The baseline technique for timing synchronization and symbol demodulation is a second-order data transition tracking loop (DTTL) module, which precedes the matched filter demodulator. The scheme implemented for the evaluation of the baseline-receiver is depicted in Figure 1. It is an equivalent implementation of the current state-of-the-art receiver [7]. Particularly, the specific implementation for deep space missions (i.e., NRZ-L encoded data) can be consulted in Figure 2.

CARRIER TO NOISE POWER SPECTRAL DENSITY ESTIMATION

The baseline receiver also includes a carrier-to-noise-density-ratio (C/N_0) estimation algorithm, which provides a useful indicator in the receiver state machine and processing modules. The estimator follows the implementation in [8] (block diagram in Figure 1).

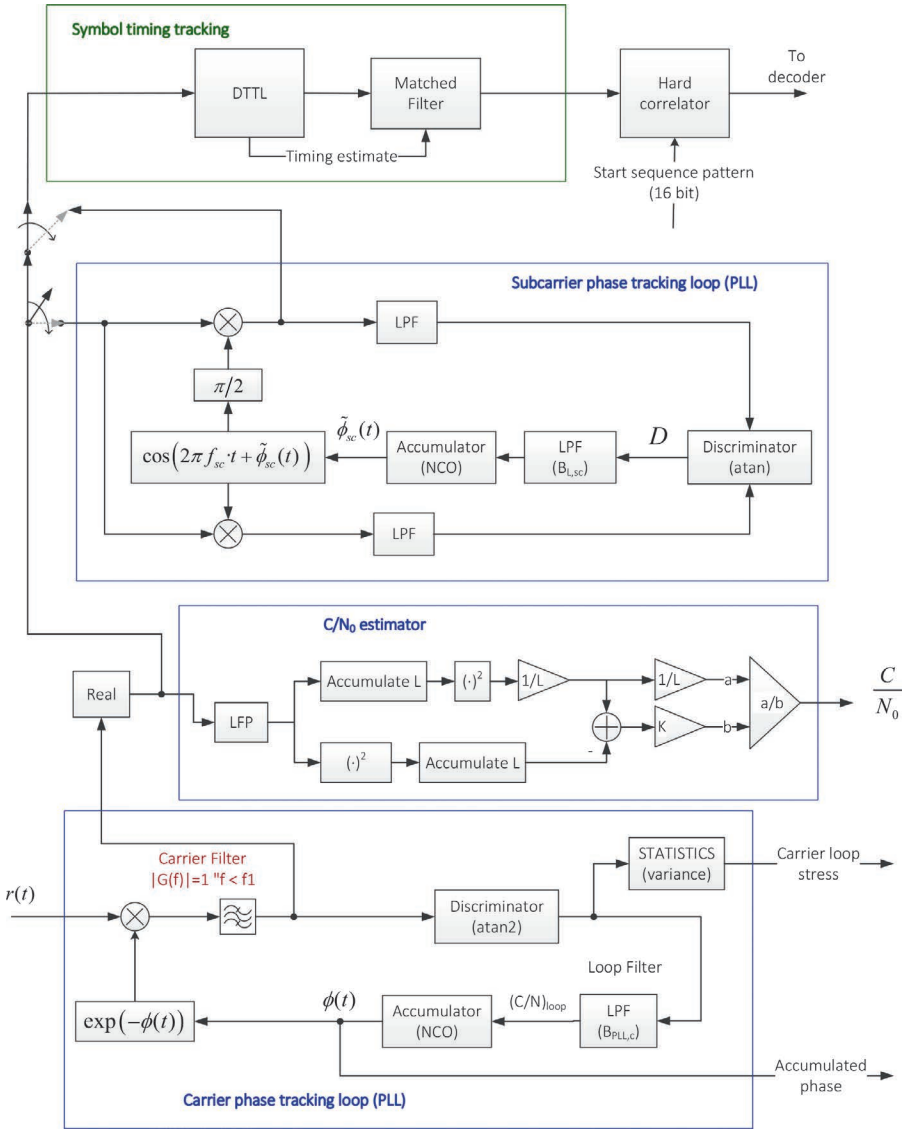

Figure 1.
Baseline receiver architecture for a deep space communications scenario.

BASELINE DEEP SPACE RECEIVER PERFORMANCE ANALYSIS

In this section we present the performance analysis of the baseline receiver architecture described in the previous section.

We consider a transmitter that generates a binary data structure, followed by the discrete-time modulator that generates the digital signal waveform samples transmitted through the channel. The channel emulator includes additive white Gaussian noise. Notice that for the assessment of the synchronization algorithms it is not necessary to implement the specific Transfer Frame data structure or the error control field of 16 parity bits [9], [10]. It is sufficient to generate a random binary vector and apply the randomizer to ensure the equivalent bit transition conditions. Throughout the article we set the receiver target operation point to $E_s/N_0 \geq 2$ with WER $\leq 10^{-5}$. Notice that E_s refers to the energy of coded symbols, which for channel coding rates of 1/2 leads to the relation $E_s/N_0 = E_b/N_0 - 3$ dB.

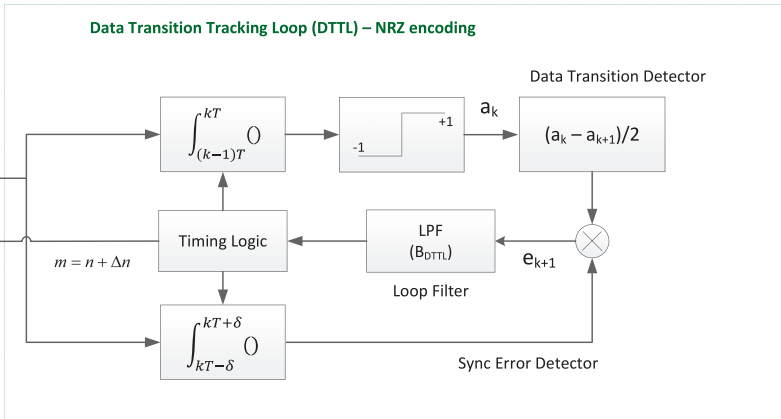

Figure 2.
DTTL symbol timing tracking for NRZ-L PCM encoding.

ACQUISITION

Before introducing the simulation results on carrier acquisition, we first provide a simple preliminary assessment in order to gain insight into the performance limits of the carrier acquisition performance. Under this setup, the C/N_0 takes the form

$$\frac{C}{N_0} = \frac{E_s}{N_0} R_s \alpha, \tag{9}$$

with $\alpha = J_0^2(m_c) \Big/ \left(2J_1^2(m_c)\right)$. The results obtained for a modulation index $m_c = 1.2$ are shown in Table 2. Taking into account the loop filter bandwidth B_L, we can define the carrier-to-noise ratio as $C/N = C/(N_0 * B_L)$, with N the noise power. Considering that the recommended value for C/N shall be equal or higher than 10 dB for a correct carrier acquisition and tracking, one can deduce that the deep space scenarios under consideration present real challenges for low E_s/N_0 values (< 4 dB) at low symbol rates, even for very narrow loop bandwidths.[2] Employing symbol rates as low as 7.125 sps may be required, for instance, in environments of limited visibility due to tumbling or other attitude issues.

Considering specific loop bandwidths and imposing the constraint $C/N \geq 10$ dB, Figure 3 shows for which symbol rates it will not be possible to successfully acquire and track the carrier. The solid red line indicates the $E_s/N_0 = 2$ dB threshold.

[2] $J_k(z)$ denotes the kth Bessel function of the first kind.

Table 2.

C/N_0 (dB – Hz) for Deep Space Scenarios as a Function of E_s/N_0 (dB)							
R_s [sps]	E_s/N_0 [dB]						
	–6	–4	–2	0	2	4	6
4,000	29.6	31.6	33.6	35.6	37.6	39.6	41.6
2,000	26.59	28.59	30.59	32.59	34.59	36.59	38.59
1,000	23.58	25.58	27.58	29.58	31.58	33.58	35.58
500	20.57	22.57	24.57	26.57	28.57	30.57	32.57
250	17.56	19.56	21.56	23.56	25.56	27.56	29.56
125	14.55	16.55	18.55	20.55	22.55	24.55	26.55
62.5	11.54	13.54	15.54	17.54	19.54	21.54	23.54
31.25	8.52	10.52	12.52	14.52	16.52	18.52	20.52
15.625	5.51	7.51	9.51	11.51	13.51	15.51	17.51
7.8125	2.5	4.5	6.5	8.5	10.5	12.5	14.5

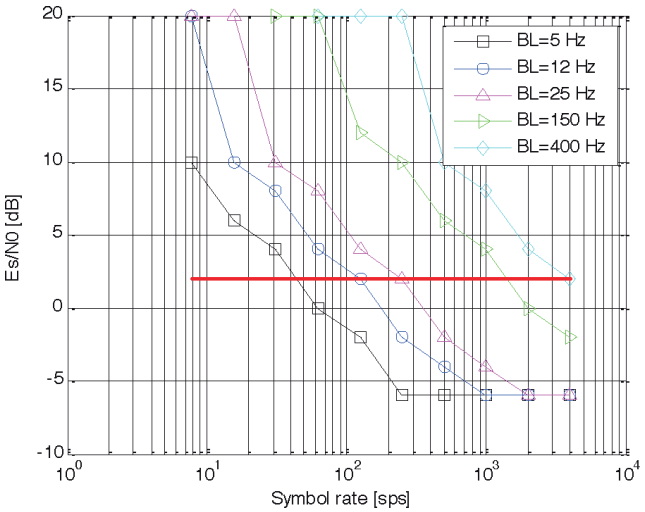

Figure 3.
Estimated required E_s/N_0 to ensure $C/N \geq 10$ dB as a function of symbol rate and loop bandwidth.

Next, we discuss the simulation results for the carrier acquisition based on the on-ground sweeping. The emulation of the on-ground sweeping is implemented by generating a data stream of an unmodulated carrier. The implementation follows the standard recommendation [6] by implementing a symmetric triangular carrier sweeping from f_{min} to f_{max}. The acquisition process must ensure the carrier sweeping passes twice through the resting frequency of the transponder PLL. As already pointed out, it has been found via simulation that carrier sweeping is not reliable for the deep space scenarios considered in this work, leading to the need for receiver enhancements (i.e., discussed in "Standard Receiver Enhancements").

CARRIER/SUBCARRIER TRACKING

In this section, we assess the performance of the carrier/subcarrier tracking stage of the receiver. The most challenging scenario corresponds to the lowest symbol rate. That is, $R_s = 7.8125$. However, the system may operate up to 4 ksps. In this analysis, both carrier and subcarrier phase tracking have been found to be a bottleneck for deep space scenarios, being impossible with the baseline receiver architecture to operate at the target $E_s/N_0 = 2$ dB and symbol rate $R_s = 7.8125$ sps. Several tests have been performed to obtain the receiver operation point limit, which mainly depends on the Doppler rate on the carrier and the residual Doppler on the subcarrier, and is directly related with the well-known noise reduction versus dynamic range trade-off. To determine such performance limits the following procedure was considered:

1. *Carrier phase tracking performance limit*. First, several tests were conducted for different symbol rates to see if the carrier phase tracking stage converged to a steady-state regime, using the carrier phase root mean square error (RMSE) and reference lock to decide if the PLL is correctly working or not. From this analysis the minimum symbol rate for each SNR was already determined.
2. *Subcarrier phase tracking performance limit*. Then, using the same reasoning, it was obtained for several case studies which was the subcarrier tracking E_s/N_0 versus R_s limit, using the RMSE in the steady-state regime and the Costas reference lock. It was found that the subcarrier tracking stage was always more restrictive (i.e., higher symbol rate required) than the carrier tracking stage; therefore, this block is the main driver on the overall system performance for a noncoherent subcarrier architecture.

Using the subcarrier performance limit, which is the most restrictive, it was verified that the symbol error rate obtained using the whole receiver chain, including the DTTL, was correct. From these results the baseline receiver performance limits were determined. The target scenario considers a Doppler rate on the carrier equal to 30 Hz/s and a residual subcarrier Doppler equal to 1 Hz. Under these conditions, the lowest symbol rate to guarantee performance at $E_s/N_0 = 2$ dB corresponds to 500 sps. If the Doppler constraints in both the carrier and subcarrier are relaxed (i.e., carrier Doppler = 1 Hz/s and subcarrier Doppler = 0.1 Hz), the system may work down to 125 sps. We summarize the main findings on the baseline receiver performance limits in Table 3.

From the different results obtained during the baseline receiver performance limits analysis, it is worth highlighting the following remarks: (i) reducing the carrier Doppler rate (for a fixed subcarrier Doppler equal to 1 Hz) does not significantly improve the receiver performance, being the Doppler on the subcarrier the main driver on the system error; and (ii) considerably reducing the Doppler on the subcarrier (i.e., from 1 Hz to 0.1 Hz) the receiver performance improvement is marginal. Then, we conclude that:

- Using enhanced carrier tracking architectures such as a third order PLL, a Kalman filter, or a FLL-assisted PLL, the expected performance gain is marginal if a noncoherent subcarrier architecture is considered.
- Considering enhanced tracking strategies such as a FLL-assisted PLL into the subcarrier, the expected performance gain is also minor. At the limit, the bottleneck on the system performance is now the carrier tracking stage.
- If both receiver enhancements are coupled, at the target $E_s/N_0 = 2$ dB the lower bound on the symbol rate for a correct

Table 3.

Baseline Receiver Lowest Symbol Rate Versus Required E_s/N_0 for a Deep Space Scenario, Considering a Subcarrier Doppler = 1 Hz and a Carrier Doppler Rate = 30 Hz/s

	E_s/N_0 [dB]					
	2	4	6	8	10	12
[sps]	500	125	62.5	31.25	15.125	7.8125

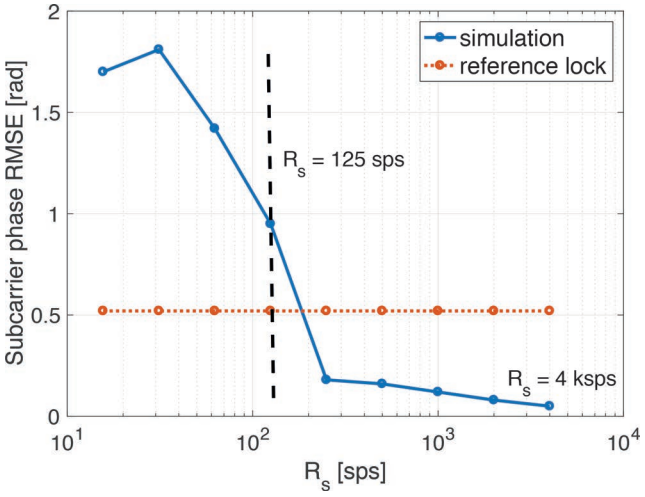

Figure 4.
Subcarrier phase RMSE versus symbol rate for the deep space scenario. Carrier Doppler rate = 1 Hz/s, subcarrier Doppler = 0.1 Hz, B_{pll} = 5 Hz, B_{Costas} = 5 Hz.

receiver (i.e., baseline receiver with noncoherent subcarrier) performance is obtained at 125 sps.

The last statement is supported by the simulation results in Figure 4, which shows the subcarrier RMSE obtained with a perfect initial acquisition, a quasi-perfect carrier tracking, and a very low subcarrier Doppler. Even with such benign conditions, the subcarrier tracking limit appears at 125 sps.

DATA TRANSITION TRACKING LOOP (DTTL) ANALYSIS

The baseline receiver symbol synchronization is performed with a DTTL. The results discussed in the previous section were obtained with the corresponding DTTL being operative and considering a correct symbol timing initialization. Here we extend the results to the case of steady-state performance. That is, assuming perfect carrier and subcarrier tracking, and a correct DTTL initialization ensuring that no error propagation comes from previous stages. The performance results are shown in Figure 5, where the symbol error rate (SER) is evaluated for different symbol rates. Clearly, at the lowest symbol rate R_s = 7.8125 sps, the SER follows the theoretical performance, showing a DTTL correct operation.

Additionally, the symbol error rate obtained with an initial symbol synchronization error equal to $T/4$ is compared to the steady-state performance results in Figures 6 and 7. Two different symbol rates were considered: (i) R_s = 500 sps, being the performance limit of the baseline receiver for the noncoherent subcarrier architecture, and (ii) R_s = 62.5 sps, being the performance limit for the coherent subcarrier architecture (see "Standard Receiver Enhancements"). In both cases the DTTL correctly synchronizes within the 128 bits acquisition sequence, indicating that the DTTL is not a bottleneck.

STANDARD RECEIVER ENHANCEMENTS

From the previous analysis of the baseline receiver, it has been found that carrier and subcarrier tracking are a bottleneck for the

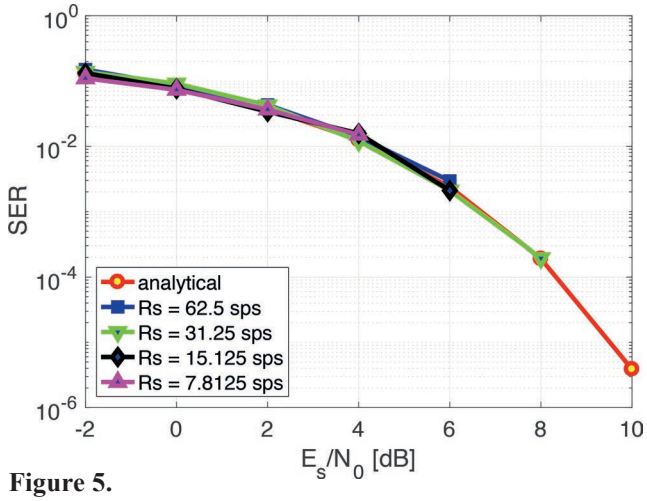

Figure 5.
SER for different symbol rates considering perfect carrier and subcarrier tracking, and correct DTTL initialization.

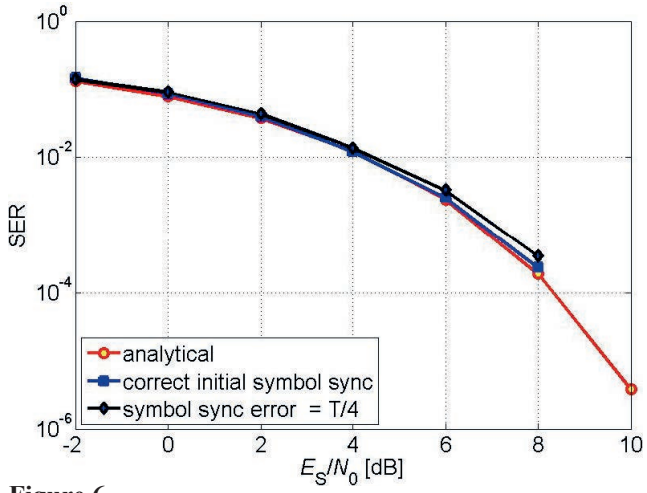

Figure 6.
SER for R_s = 500 sps considering perfect carrier and subcarrier tracking, and two DTTL initializations: correct symbol sync and initial symbol sync error = $T/4$.

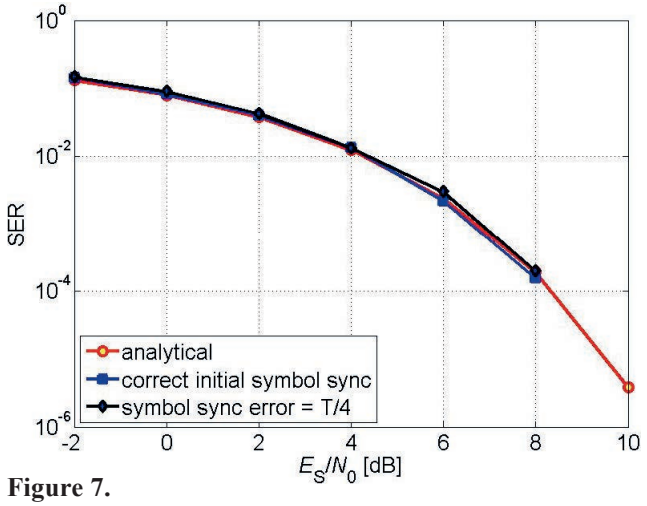

Figure 7.
SER for R_s = 62.5 sps considering perfect carrier and subcarrier tracking, and two DTTL initializations: correct symbol sync and initial symbol sync error = $T/4$.

deep space scenario at the target $E_s/N_0 = 2$ dB, for the lowest symbol rates. In this section we consider some receiver enhancements to overcome the limitations of the standard architecture and analyze their performance.

One of the main challenges for proper receiver operation at the extremely low signal-to-noise ratio is to reduce the noise contribution to the tracking loops, which requires reducing the loop bandwidth as much as possible. This is in contrast to having a sufficiently large loop bandwidth to increase the pull-in range and allow signal lock. An enhancement aimed at reducing the loop bandwidth at the tracking loops is to improve the acquisition of the corresponding signal; namely, improving the estimate of the resting frequency of the baseline carrier and subcarrier tracking loops, PLL and Costas loops, respectively. To this end, it is known that FFT techniques are an alternative to acquire the carrier (or subcarrier) frequency deviations and therefore correct them.

FFT-BASED CARRIER ACQUISITION

In order to reduce the bandwidth of the PLL (or the desired scheme used to track the carrier phase), an FFT can be used to accurately estimate the Doppler shift of the carrier and correct for it at the loop's Numerically-Controlled Oscillator (NCO), in which case sweeping from the ground is not required. The precision of this technique can be adjusted, depending basically on the number of points used in the FFT computation.

In order to validate the implementation and show the performance of FFT-based carrier tracking acquisition schemes, a set of experiments were conducted, where several FFT points were tested. For each experiment, we average the carrier frequency and carrier phase RMSE over time for different E_s/N_0 values. It is clear that increasing the FFT size has a notable impact on the ability of the receiver to lock the carrier signal. Therefore, this technique is very interesting, particularly in scenarios with low SNR at the receiver input.

The evaluation is shown for $R_s = 62.5$ sps, which corresponds to the lowest symbol rate that can achieve the target performance at $E_s/N_0 = 2$ dB. Since, for the deep space telecommand scenario, we have very low symbol rates, the FFT-aided carrier acquisition technique is very challenging. The results illustrate how the different configuration parameters affect the performance. The main parameter affecting performance is the number of FFT points (i.e., between 512 and 8,192), since it determines the accuracy of the frequency estimate. The frequency resolution or frequency bin width is given by the sampling frequency (which is adjusted to the frequency span where the Doppler shift is expected) used by the FFT computation and the number of FFT points. To evaluate this effect, we have considered three different Doppler spans: 500 Hz, 5 kHz, and 100 kHz. For each scenario, each Monte-Carlo realization randomly generates the Doppler shift between 0 and the Doppler span. The second parameter is the number of FFT blocks (number of performed FFTs) used to estimate the periodogram (i.e., 1 to 10 averaged FFT blocks). Increasing the number of FFT blocks reduces the variance of the estimated periodogram. Besides the constraints on memory and processing power the transponder architecture may impose, the maximum number of FFT blocks is determined by the channel coherence.

For instance, for the lower Doppler span of 500 Hz, 512-point FFT results in a frequency bin of approximately 2 Hz. However, when the Doppler span is 100 kHz we need to increase the number of FFT-points to 8,192 to obtain a similar frequency bin resolution. We summarize the FFT related parameters in Table 4.

The results obtained in several configurations for demanding scenarios are shown in Table 5. We declare a *misacquisition* the

Table 4.

FFT Related Parameters

Maximum Doppler Shift	FFT Sampling Frequency	FFT Size	Frequency Bin	Doppler Shift in an FFT Block	Maximum Number of FFT Blocks
500 Hz	1 kHz	512	1.95 Hz	7.68 Hz	1
		1,024	0.97 Hz	15.36 Hz	1
		512	19.53 Hz	0.76 Hz	25
		1,024	9.76 Hz	1.53 Hz	6
5,000 Hz	10 kHz	2,048	4.88 Hz	3.07 Hz	1
		4,096	2.44 Hz	6.14 Hz	1
		8,192	1.22 Hz	12.3 Hz	1
		512	390.62 Hz	0.04	> 10,000
		1,024	195.31 Hz	0.08 Hz	> 2,500
100 kHz	200 kHz	2,048	97.65 Hz	0.15 Hz	635
		4,096	48.82 Hz	0.31 Hz	159
		8,192	24.41 Hz	0.61 Hz	39

cases where the error is much larger than the frequency resolution (> 100 Hz, in which cases the PLL is not able to lock) and compute the RMSE over the successful acquisition realizations. We can conclude that the FFT approach enables successfully acquisition of the carrier frequency for a large Doppler span without the need for carrier sweeping, thus enabling narrowing of the PLL loop bandwidth for successful lock at low E_s/N_0 (or equivalently low C/N_0).

FFT-AIDED SUBCARRIER TRACKING

The concept is similar to the one applied for the carrier frequency acquisition. An FFT is applied to determine, with adjustable precision, the Doppler deviation on the subcarrier frequency. Then, this estimate is used to improve the resting frequency of the baseline Costas loop. By doing so, the loop bandwidth can be further reduced, thus being able to operate at lower SNR values. Figure 8 depicts the block diagram of the subcarrier tracking including this enhancement. Besides the number of FFT points, in order to increase the precision of this technique, downsampling can be also used.

The same analysis conducted in the previous section has been done also for the third order PLL + Costas-FFT + DTTL case, with the main results summarized in Table 6. Comparing these results with the performance limits obtained for the baseline receiver architecture, it is clear that using the FFT for better initialization of tracking loops improves the system performance by lowering the required E_s/N_0 from 12 to 10 dB. However, it is still far from the 2 dB target.

Table 5.

Results for the FFT-Aided Carrier Acquisition for a Deep Space Scenario

E_s/N_0 [dB]	10		6		4		2	
Results for 500 Hz								
FFT size/blocks	512/1		512/1		512/1		512/1	
Number of realizations	50		50		50		50	
Number of misacquisitions	2		6		5		7	
RMSE	5.33 Hz		5.31 Hz		5.55 Hz		5.48 Hz	
RMSE (including failures)	77.55 Hz		104.88 Hz		109.81 Hz		107.36 Hz	
Results for 5 kHz								
FFT size/blocks	512/10	8,192/10	512/10	8,192/10	512/10	8,192/10	512/10	8,192/10
Number of realizations	50	50	50	50	50	50	50	50
Number of misacquisitions	13	14	13	13	14	17	13	15
RMSE	17.9 Hz	8.07 Hz	18.19 Hz	9.14 Hz	18.79 Hz	8.65 Hz	16.79 Hz	8.06 Hz
RMSE (including failures)	1.38 kHz	1.56 kHz	1.19 kHz	1.36 kHz	1.71 kHz	1.57 kHz	1.34 kHz	1.82 kHz
Results for 100 kHz								
FFT size/blocks	8,192/1	8,192/10	8,192/1	8,192/10	8,192/1	8,192/10	8,192/1	8,192/10
Number of realizations	50	50	50	50	50	50	50	50
Number of misacquisitions	3	0	35	0	43	0	46	3
RMSE	22.96 Hz	23.67 Hz	19.28 Hz	22.70 Hz	19.86 Hz	24.57 Hz	19.81 Hz	21.89 Hz
RMSE (including failures)	31.58 kHz	23.67 Hz	76.31 kHz	22.70 Hz	89.32 kHz	24.57 Hz	83.48 kHz	5.78 kHz

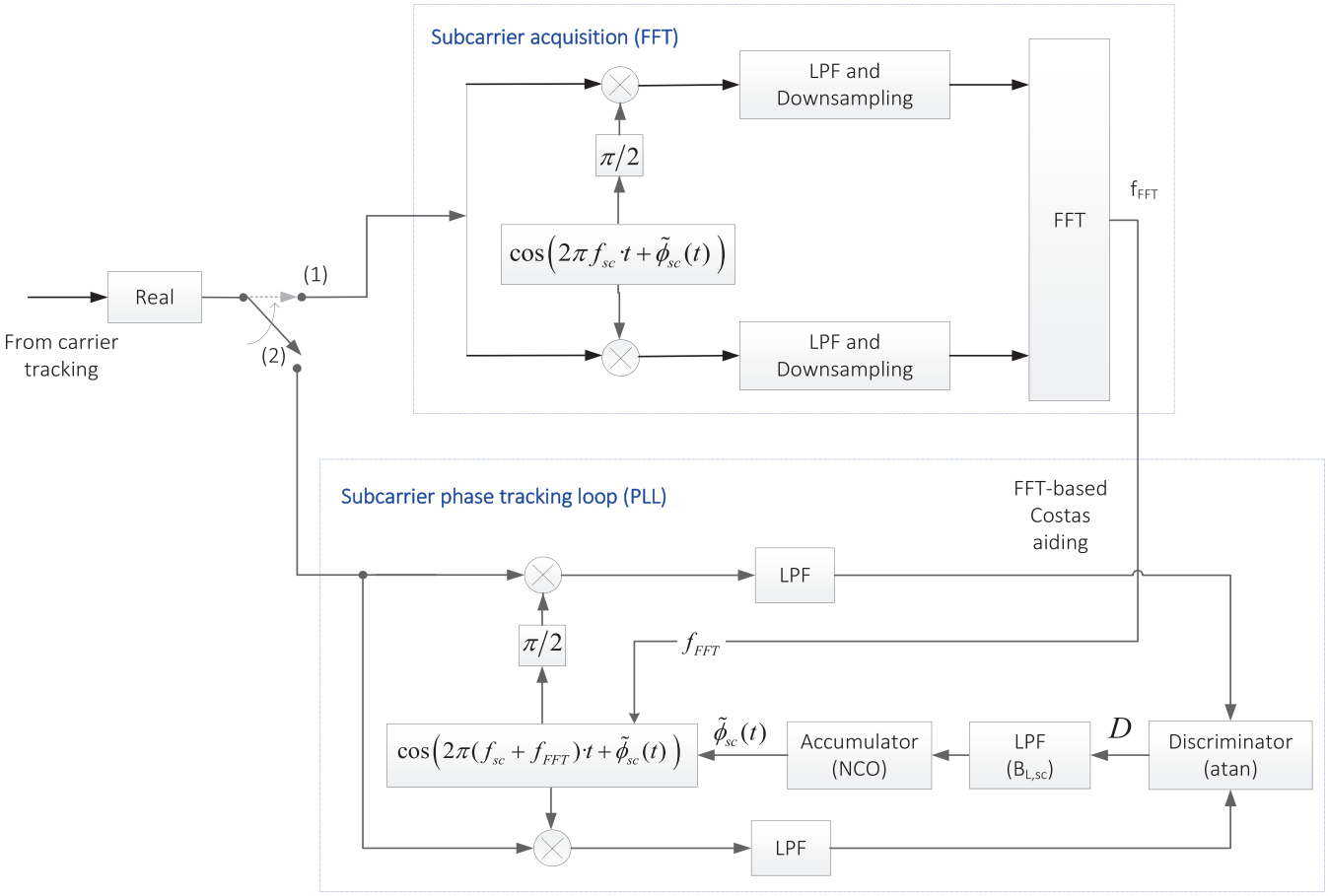

Figure 8.
FFT-aided Costas loop. An FFT is used to acquire the Doppler on the subcarrier and then a standard Costas loop is used, whose resting frequency is corrected by f_{FFT}.

FLL-ASSISTED PLL AND KF-BASED CARRIER TRACKING SCHEMES

We have seen that the carrier tracking in the baseline receiver, performed with a second order PLL, is compromised in the considered deep space scenarios by the noise reduction versus dynamic range trade-off. That is, the PLL has to operate at very low SNR, which implies using a very narrow bandwidth, but the incoming signal is affected by a moderate carrier Doppler rate, being more suitable to cope with such dynamics to increase the loop bandwidth. As a result, the filter is not able to meet both requirements and loop does not lock to the incoming signal's carrier phase. To overcome these limitations two techniques are considered: (i) *FLL-assisted PLL* and (ii) *Kalman filter-based carrier tracking*. For both methods we assume an FFT-based carrier acquisition, and the subcarrier tracking is evaluated considering the FFT-aided Costas loop to improve the acquisition and tracking in the presence of residual Doppler in the subcarrier.

The FLL-assisted PLL is investigated in order to be able to reduce the PLL bandwidth while keeping track of the Doppler dynamics. The main idea is to use a second order FLL to sequentially estimate the signal's frequency, which is then fed to a third order PLL. In this case, the PLL has to cope with a reduced dynamics signal, being able to use a lower bandwidth and improving the noise reduction. From the results obtained, the FLL is not performing correctly at low SNR, therefore the frequency aiding is not improving the standalone PLL performance for the target scenarios. The fact that the FLL-assisted PLL carrier tracking is not robust to low SNR is well known in the literature, because the FLL discriminators are much more sensitive to noise (compared to phase discriminators) due to the inherent noise amplification. This is the reason why these schemes are usually discarded to operate at low SNR and are not of interest in this study.

Table 6.

Third Order PLL + Costas-FFT + DTTL Performance Limits for a Deep Space Scenario, Considering a Subcarrier Doppler Initialized with the FFT and a Carrier Doppler rate = 30 Hz/s

	E_s/N_0 dB				
	2	**4**	**6**	**8**	**10**
[sps]	125	62.5	31.25	15.125	7.8125

It has been shown in the literature that the standard PLL limitations are usually overcome by KF-based carrier tracking solutions. It is well known that a standalone PLL is equivalent to a KF with a priori fixed gain (i.e., fixed bandwidth); therefore, it is expected that a KF performs at least as well as its PLL counterpart. One of the main advantages of the KF in its standard form is that the Kalman gain is sequentially and optimally computed, which can be seen as an inherent adaptive bandwidth of the filter. The time-varying Kalman filter gain is the equivalent of the constant PLL loop filter coefficients, and the state prediction acts as an integrator, being equivalent to the NCO block in the standard PLL. The optimal bandwidth computation performed by the KF significantly increases the computational complexity and the required system knowledge when compared to the simplicity of the PLL, where only the loop bandwidth must be specified. That is the reason why the latter is still considered the method of choice in many applications.

We show in Figure 9 the standard adaptive KF (i.e., adaptive referring to the adaptive computation of the discriminator phase noise variance from the sequential C/N_0 estimation) carrier phase RMSE, obtained for the R_s = 125 sps, compared to the second and third order PLLs. Although the performance gain obtained with the adaptive KF is clear from the results in this case study, the computational complexity is significantly higher and the filter tuning much more complex than for the standard PLL, where only the bandwidth and order of the filter are specified [5]. The adaptive bandwidth behavior of the KF is shown in Figure 10.

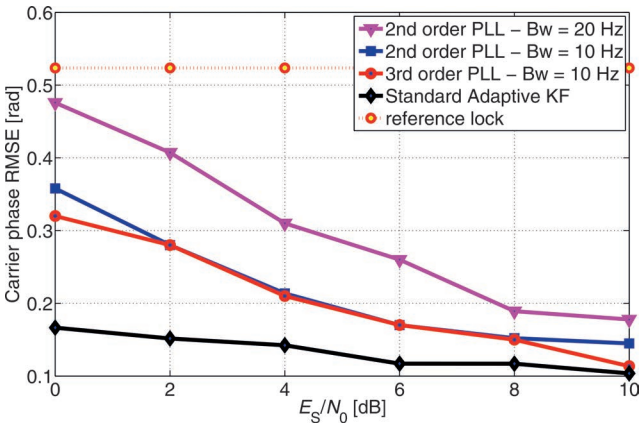

Figure 9.
Carrier tracking performance for R_s = 125 sps, considering a standard adaptive KF, second, and third order PLLs.

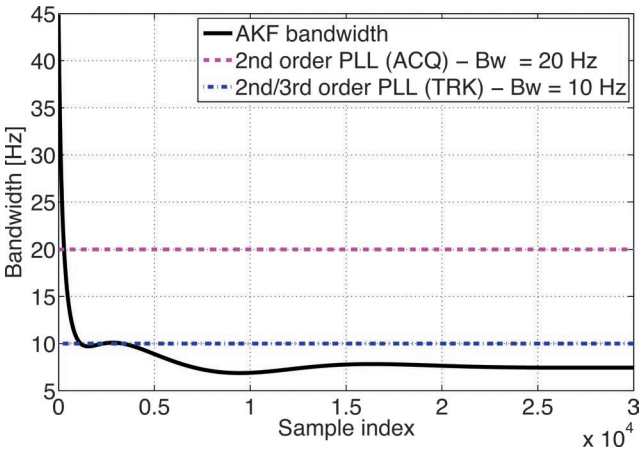

Figure 10.
Adaptive KF bandwidth versus constant PLL bandwidth.

COHERENT CARRIER/SUBCARRIER TRACKING

The solution to overcome and improve the limitations of noncoherent carrier/subcarrier tracking approaches and go below the R_s = 125 sps achieved with the enhanced FFT-based Costas subcarrier tracking, is to consider a coherent carrier/subcarrier architecture.

Even evaluating the baseline receiver assuming a subcarrier Doppler of 0 Hz (i.e., coherent carrier/subcarrier), the system cannot operate at the lowest symbol rate. However, good performance is achieved for R_s = 62.5 sps, which considerably improves performance with regard to the FFT-aided Costas loop. Yet, the required E_s/N_0 = 10 dB to be able to operate at R_s = 7.8125 sps. Table 7 summarizes the results. In this case, the main driver on the receiver performance limit is no longer the subcarrier (i.e., the Costas bandwidth can be reduced from 15 Hz to 2 Hz) but the carrier tracking stage.

The simulated SER is compared in Figure 11 for different symbol rates. These results confirm the performance limits shown in

Table 7.

Baseline Receiver Performance Limits for a Coherent Subcarrier, Subcarrier Doppler = 0 Hz and Carrier Doppler Rate =30 Hz/s				
	E_s/N_0 dB			
	2	4	6	10
[sps]	62.5	31.25	15.125	7.8125

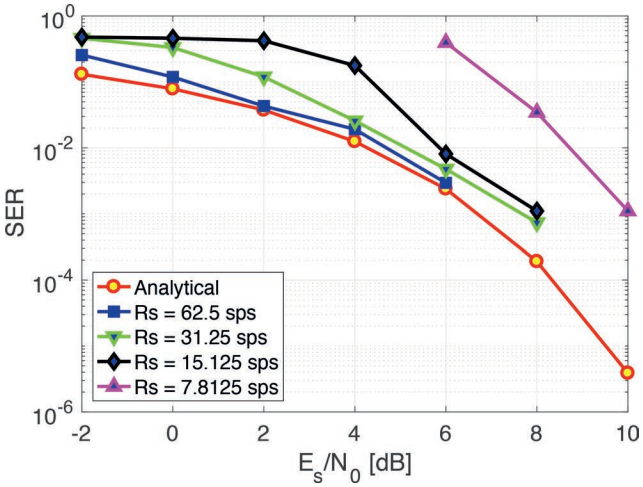

Figure 11.
SER performance for the deep space scenario considering a third order PLL + Costas, and a coherent subcarrier.

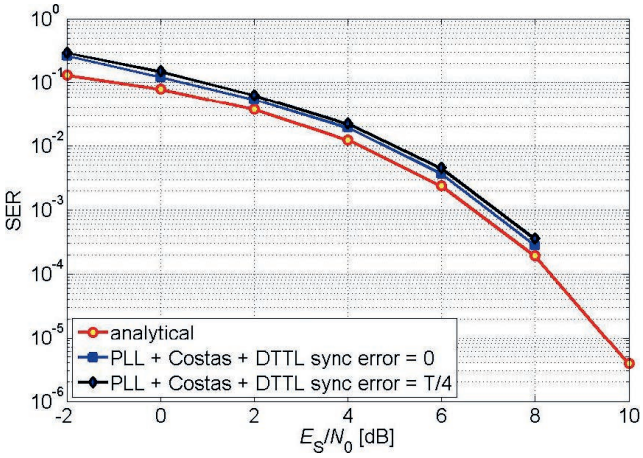

Figure 12.
SER performance for the deep space scenario considering a third order PLL + Costas architecture, and a coherent subcarrier for R_s = 62.5 sps.

Table 7 and are in line with the results obtained for the FFT-based Costas scheme.

To complete the analysis and characterization of the coherent carrier/subcarrier architecture, the DTTL performance (considering the SER for the whole receiver chain) with a correct timing synchronization initialization is compared to the case where the initial synchronization error = $T/4$ in Figure 12. Note that the same results are valid for other timing initializations. As was shown in the standalone DTTL performance analysis, the performance obtained with both perfect and imperfect initializations is equivalent.

NONCOHERENT TIMING SYNCHRONIZATION

An alternative approach to improve the overall receiver architecture performance is the Noncoherent DTTL (NC-DTTL). The main idea of the NC-DTTL is to avoid the subcarrier tracking stage by using a noncoherent architecture, which is shown in Figure 13. Notice that even if the subcarrier tracking stage is avoided, the input to the NC-DTTL is the output of the carrier tracking stage (i.e., PLL); therefore, the limitations of this first stage are not solved with such architecture. In other words, using a coherent subcarrier, it has been shown that the third order PLL performance limit at E_s/N_0 = 2 dB is given by the R_s = 62.5 sps case; thus, using the NC-DTTL the performance limit is the same.

The steady-state performance comparison of the NC-DTTL with the standard DTTL for the coherent architecture and R_s = 62.5 sps is shown in Figure 14, where again it is clear that the performance obtained with both architectures is equivalent.

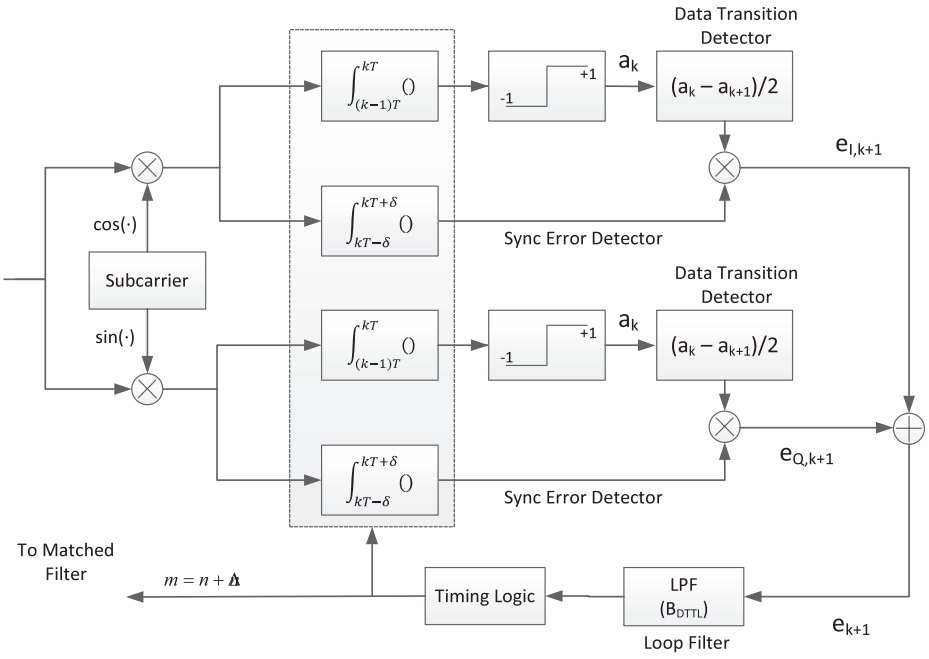

Figure 13.
Noncoherent DTTL.

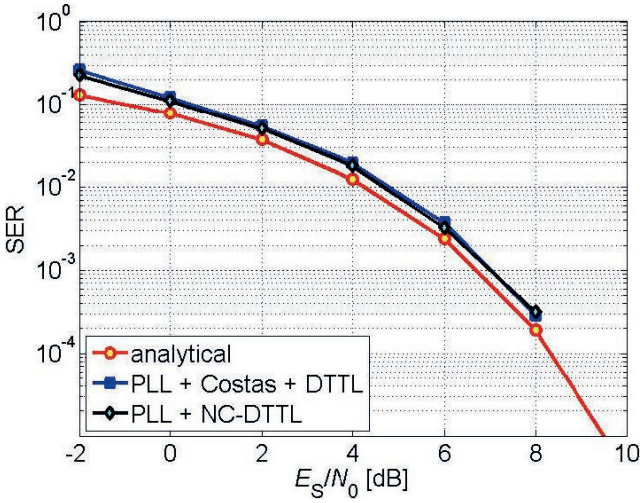

Figure 14.
DTTL versus NC-DTTL considering a coherent subcarrier and R_s = 62.5 sps.

CONCLUSIONS

An assessment of the baseline baseband receiver functionalities has been carried out, supported by performance simulations based on a detailed link level simulation software model. The following bottlenecks are identified:

1. Carrier acquisition (performed on the unmodulated carrier signal) does not represent a bottleneck for sufficiently high C/N_0. For deep space scenarios, the carrier sweeping limits the performance at low symbol rate at the target E_s/N_0 = 2 dB. An enhanced carrier acquisition scheme based on spectral estimation techniques (it requires FFT processing, averaging, and simple threshold detec-

tion) can relax the requirements on the carrier loop enforced by the on-ground sweeping procedure. Such an approach has several advantages: (i) FFT-based carrier acquisition does not require on-ground sweeping, (ii) allows faster acquisition, and (iii) can reach lower estimation errors on carrier frequency.

2. Carrier and subcarrier tracking are the critical bottleneck in order for the receiver to operate at the target E_s/N_0 for the selected deep space scenarios. From the evaluated enhanced approaches, FFT-aided Costas subcarrier acquisition and tracking provides gains in the low SNR region, yet they do not meet the target E_s/N_0 at the low rate scenario.

3. An alternative solution that affects the transmitter side, which implies implementing a coherent carrier and subcarrier generation, would significantly improve the receiver synchronization performance. In this line, a noncoherent demodulation that avoids subcarrier tracking has been evaluated, showing promising results. The noncoherent scheme is compared to the coherent receiver that performs subcarrier tracking by means of a Costas loop and the same symbol timing tracking and demodulation scheme. Both schemes achieve very similar performance. The former avoids subcarrier tracking but requires implementing two DTTL branches.

To summarize, the assessment of the code impact on the receiver functionalities and identification of bottlenecks in the transponder synchronization schemes indicate that both acquisition and tracking loops must be upgraded to fully exploit the potential gains that more powerful coding schemes bring to telecommand in space communications. Current standard configurations will not be able to operate at the lower link budget for the lowest rate operational modes. ◈

ACKNOWLEDGMENTS

This work has been supported by the Spanish Ministry of Economy and Competitiveness through project TEC2015-69868-C2-2-R (ADVENTURE), ESA's Basic Technology Research Programme entitled Next Generation Uplink Coding Techniques (NEXCODE), Contract No. 4000111690/14/NL/FE, and by the Government of Catalonia under Grant 2014–SGR–1567.

REFERENCES

[1] Baldi, M., Bertinelli, M., Chiaraluce, F., Closas, P., Dhakal, P., Garello, R. et al. State-of-the-art space mission telecommand receivers. *IEEE Aerospace and Electronic Systems Magazine,* Vol. 32, 6 (2017), 4–15.

[2] CCSDS. Next generation uplink. green book, CCSDS 230.2-G-1. Jul. 2014.

[3] Baldi, M., Bertinelli, M., Chiaraluce, F., Closas, P., Garello, R., Maturo, N. et al. Nexcode: Next generation uplink coding techniques. In *Proceedings of the 7th ESA International Workshop on Tracking, Telemetry and Command Systems for Space applications (TT&C)*, Estec, Noordwijk, The Netherlands, Sep. 2016.

[4] Pfletschinger, S., Navarro, M., and Closas, P. Frame synchronization for next generation uplink coding in deep space communications. In *Proceedings of the IEEE Global Communications Conference, Exhibition & Industry Forum (GLOBECOM 2015)*, San Diego, CA, Dec. 2015.

[5] Vilà-Valls, J., Closas, P., Navarro, M., and Fernández-Prades, C. Are PLLs dead? A tutorial on Kalman filter-based techniques for digital carrier synchronization. *IEEE Aerospace & Electronic Systems Magazine,* Vol. 32, 7 (2017), 28-45.

[6] ECSS. Radio frequency and modulation. ECSS-E-ST-50-05C Rev.2, Oct. 2011.

[7] Hamkins, J., and Simon, M. K. *Autonomous Software-Defined Radio Receivers for Deep Space Applications*. New York: Wiley, 2006.

[8] Monk, A. M. Carrier-to-noise power estimation for the block V receiver. JPL TDA Progress Report 42 (1991): 106, Tech. Rep., Oct. 1991.

[9] ECSS. Space data links—Telecommand protocols, synchronization and channel coding. ECSS-E-ST-50-04C, Jul. 2008.

[10] CCSDS. TC synchronization and channel coding, blue book. CCSDS 231.0-B-3, Sep. 2017.